NeuroImage 200 (2019) 562–574

Contents lists available at ScienceDirect

NeuroImage

journal homepage: www.elsevier.com/locate/neuroimage

Corresponding anatomical and coactivation architecture of the human precuneus showing similar connectivity patterns with macaques

Jiaojian Wang [a,*], Benjamin Becker [a], Lijie Wang [a], Hai Li [b,c], Xudong Zhao [d], Tianzi Jiang [a,b,c,e,f,**]

[a] Key Laboratory for Neurolnformation of Ministry of Education, School of Life Science and Technology, University of Electronic Science and Technology of China, Chengdu, 625014, China
[b] Brainnetome Center, Institute of Automation, Chinese Academy of Sciences, Beijing, 100190, China
[c] National Laboratory of Pattern Recognition, Institute of Automation, Chinese Academy of Sciences, Beijing, 100190, China
[d] State Key Laboratory of Brain and Cognitive Science, Institute of Biophysics, Chinese Academy of Sciences, Beijing, 100101, China
[e] CAS Center for Excellence in Brain Science and Intelligence Technology, Institute of Automation, Chinese Academy of Sciences, Beijing, 100190, China
[f] University of Chinese Academy of Sciences, China

ARTICLE INFO

Keywords:
Precuneus
Anatomical connectivity
Coactivation
Parcellation
Macaque

ABSTRACT

The precuneus (PCun) is one of the most expanded areas of the association cortex and plays an important role in integrating information from different modalities. However, whether the functional architecture of PCun is shared by humans and macaques is an open question. We used both anatomical connectivity and task-dependent coactivation patterns to parcellate the human PCun and consistently identified three subregions in the human PCun using two independent datasets. Two subregions were located in the dorsal PCun and one subregion was located in the ventral PCun. This parcellation scheme for the PCun was supported by identifying the subregion-specific networks and by functional characterization. Then, the absolute and relative gray matter volume of precuneus in human and macaque was calculated and significantly smaller absolute and relative gray matter volume in macaque was identified. Next, three macaque PCun subregions were defined based on our tractographic atlas. Finally, the whole brain anatomical connectivity patterns and connectivity fingerprints with 17 predefined homologous target brain areas were mapped for each PCun subregion and revealed that the PCun shares similar anatomical connectivity patterns in humans and macaques. The similar anatomical connectivity patterns of PCun were validated by an independent in-house dataset. Our findings demonstrated that anatomical connectivity patterns can reflect the functional architecture of the PCun in humans and that the functional architecture of the PCun is similar in humans and macaques.

1. Introduction

The precuneus (PCun) is a functionally heterogeneous region that contributes critically to visually guided movement (Battaglia-Mayer and Caminiti, 2002; Lacquaniti et al., 1995; Marconi et al., 2001), visuospatial imagery, episodic memory retrieval, self-processing, and consciousness (Cavanna and Trimble, 2006). The engagement in different functional domains suggests that this region has a complex functional architecture and, indeed, microscopic cytoarchitectonic (Scheperjans et al., 2008a, 2008b) as well as macroscopic functional and anatomical connectivity approaches (Zhang and Li, 2012; Zhang et al., 2014) revealed distinct PCun subdivisions. However, the different parcellation schemes yielded inconsistent results, and the functional architecture of this region remains controversial. Recent studies employed multimodal analysis strategies and suggested that these integrative approaches allow determination of convergent markers across anatomical and functional modalities. In particular, anatomical connectivity patterns can predict task-specific activity, e.g. during face processing (Saygin et al., 2016) and can inform the resting-state and task-based functional organization of the parietal lobules (Wang et al., 2015b, 2017d). Such multimodal approaches thus appear particularly suitable for integrating previously reported inconsistencies between unimodal parcellation approaches and may allow researchers to reach a consensus topography of the PCun.

Previous studies have demonstrated that brain functions are

* Corresponding author.
** Corresponding author. Brainnetome Center, Institute of Automation, Chinese Academy of Sciences, Beijing, 100190, China.
E-mail addresses: jiaojianwang@uestc.edu.cn (J. Wang), jiangtz@nlpr.ia.ac.cn (T. Jiang).

https://doi.org/10.1016/j.neuroimage.2019.07.001
Received 27 March 2019; Received in revised form 3 June 2019; Accepted 1 July 2019
Available online 2 July 2019

determined by a brain region's external connectivity patterns, i.e. its connectivity fingerprints (Passingham et al., 2002). In vivo diffusion magnetic resonance imaging (MRI) can non-invasively map the whole brain white matter fiber tracts to characterize the brain anatomical connectivity patterns (Hagmann et al., 2006). Additionally, using the BrainMap database (www.brainmap.org), we can also identify the task-related whole brain coactivation patterns across a wide range of neuroimaging experiments to elucidate the brain's architecture during tasks (Clos et al., 2013; Eickhoff et al., 2011). Many previous studies have used anatomical or coactivation patterns to define fine-grained functional subregions and have shown similar topographies using microscopic cytoarchitecture-based mapping (Clos et al., 2013; Mars et al., 2011; Wang et al., 2012, 2016, 2017d; Xu et al., 2015). Moreover, a large number of studies have revealed that human brain functions were strongly related to anatomical connectivity (Deco et al., 2013, 2014; Wang et al., 2015b, 2016). Therefore, using both anatomical connectivity and a coactivation-based parcellation approach to define a consensus topography can effectively investigate brain structural and functional relationships and guide the functional mapping of the brain.

Although the macaque model has been widely used as a translational model to investigate the neural basis of basic cognition and of psychiatric disorders (Capitanio and Emborg, 2008; Gregoriou et al., 2014), similarities between the functional architecture in macaque and humans remain unknown. The human PCun is one of the last brain areas to become fully myelinated (Goldman-Rakic, 1987). Whereas the human PCun is considered to be a group of heterogenous functional subcomponents, the macaque PCun has traditionally been considered to be a single, homogenous component and is referred to as PGm or 7 m (Parvizi et al., 2006). However, using resting-state functional connectivity (RSFC) analyses of anesthetized macaque fMRI data, Margulies et al. (2009) identified different functional networks in the PCun of macaques, and these functional networks were similar in humans and macaques. Moreover, using an anatomical connectivity-based parcellation approach, we were able to identify 3 PCun subregions in macaques (Wang et al., 2018), providing further support for similarities with the human PCun architecture. However, whether the human PCun shares the same topography and connectivity patterns with the macaque remains unclear.

Our goal in the present study was to discover whether the anatomical connectivity patterns reflect the task-related architecture of the human PCun using Human Connectome Project (HCP) data and an independent in-house dataset. Furthermore, we wanted to discover whether the topological organization and anatomical connectivity patterns of the PCun are similar in humans and macaques. To achieve these goals, anatomical connectivity and coactivation-based parcellation approaches were first employed to determine a consensus structural and functional topographical organization of the PCun in humans. Subsequently, each of the PCun subregion was functionally characterized based on its RSFC patterns, task-related coactivation networks, and functional characterizations. Next, the macaque PCun subregions were defined based on our previous tractographic atlas (Wang et al., 2018). Finally, the whole brain and target-based anatomical connectivity fingerprints were mapped and compared to see whether human and macaque have similar connectivity patterns of the PCun at the sub-regional level. When similar structural and task-related functional topographies of PCun was determined in human, the similar anatomical connectivity patterns between human and macaque indicate that similar functional activity may be found in macaque. Finally, to validate the PCun parcellation in humans, an independent in-house dataset was used to try to replicate the PCun parcellation as well as the whole brain and target-based anatomical connectivity patterns for each PCun subregion.

2. Materials and methods

2.1. Human data

To independently replicate the anatomical connectivity-based parcellation of the human PCun two independent data sets were used. The first was a publicly available dataset from the Q3 data release of the Human Connectome Project (HCP). This dataset includes 40 healthy, right-handed subjects (17 males, age range = 22–35 years). The second dataset was an in-house dataset from 40 healthy, right-handed participants (20 males, age range, 17–20 years), all of whom provided written informed consent before inclusion in the study. The study was in accordance with the latest revision of the declaration of Helsinki and had full ethical approval from the local Research Ethics Committee of the University of Electronic Science and Technology of China. Both human datasets had been previously used to construct a whole brain anatomical connectivity atlas, as outlined in our previous research report (Fan et al., 2016).

2.2. Macaque data

Twenty-four healthy male adult rhesus macaques were selected from a primate research center. All the macaques enrolled in the present study were housed at the Primate Research Center at the Institute of Biophysics, Chinese Academy of Sciences. The experimental procedures adhered to approved guidelines and regulations for the National Care and Use of Animals, and the experimental protocols were approved by the National Animal Research Authority of China and the Institutional Animal Care and Committee of the Institute of Biophysics, Chinese Academy of Sciences. For detailed information on the 24 monkeys, please refer to our previous publication, which used diffusion MRI data from these animals to construct a cortical tractographic atlas (Wang et al., 2018).

2.3. MRI data acquisition – human subject

The MRI data from the HCP were acquired using a 3.0 T S MR system. The preprocessed DWI data included 270 directions with diffusion weighting consisting of 3 shells (b = 1000, 2000, and 3000 s/mm^2) and 18 non-diffusion-weighted images (b = 0 s/mm^2). The diffusion MRI data were acquired using the following parameters: TR = 5520 ms, TE = 89.5 ms, and voxel resolution = 1.25 × 1.25 × 1.25 mm^3, no gap. In addition, sagittal 3D T1-weighted images were acquired (TR/TE = 2400/2.14 ms, voxel resolution = 0.7 × 0.7 × 0.7 mm^3). For detailed information about the HCP data we refer to a previous publication by Van Essen and colleagues (Van Essen et al., 2013).

The in-house data were obtained using a 3.0 T GE MR system. The diffusion MRI data included 64 diffusion gradient (b = 1000 s/mm^2) images and 3 non-diffusion-weighted images (b = 0 s/mm^2). The following acquisition parameters were used for the diffusion MRI: acquisition matrix = 128 × 128, flip angle (FA) = 90°, voxel resolution: 2 × 2 × 2 mm^3, 75 slices. Additional sagittal 3D T1-weighted images were acquired using the following parameters: TR/TE = 8.16/3.18 ms; FA = 7°; inversion time = 800 ms; FOV = 256 mm × 256 mm; matrix = 256 × 256; slice thickness = 1 mm. To delineate the PCun subregion-specific functional networks, all the subjects also underwent a resting state scan. During the fMRI acquisition the subjects were instructed to think about nothing in particular and to keep their eyes closed without falling asleep. Cushions were used to reduce head motion. The functional data were acquired using the following parameters: TR = 2000 ms, TE = 30 ms, voxel size = 3.75 × 3.75 × 4 mm^3, no gap, 40 axial slices. A total of 255 vol were acquired.

2.4. MRI data acquisition – macaques

The macaque MRI data were collected using a 3 T S MR system. Before the scanning procedure the macaques were anesthetized with intramuscular ketamine (10–15 mg/kg) and atropine (0.05 mg/kg). Intravenous propofol induction/maintenance levels were 1 mg/kg/min. The anesthesia was stable for at least 1 h before the MRI acquisition. The macaque diffusion MRI data included 64 diffusion gradient (b = 1000 s/mm^2) images and 1 non-diffusion-weighted image (b = 0 s/mm^2). The

data were acquired using the following scanning parameters: TR/TE = 5000/95 ms, FOV = 120 mm × 120 mm, acquisition matrix = 80 × 80, FA = 90°, slice thickness = 1.5 mm. Additional sagittal-oriented 3D T1-weighted images were acquired using the following parameters: TR/TE = 2200/3.68 ms; inversion time = 760 ms; FA = 8°; FOV = 128 mm × 128 mm; matrix = 256 × 256, 224 sagittal slices, and slice thickness = 0.5 mm. For the detailed acquisition and processing procedures of the macaque MRI data please refer to our previous publication (Wang et al., 2018).

2.5. Diffusion MRI data preprocessing

The publicly available HCP data were already preprocessed; see Glasser et al. (2013) for the details. Preprocessing for the in-house and the macaque diffusion MRI data was carried out using the FSL software (http://www.fmrib.ox.ac.uk/fsl). In an initial step, the eddy currents and head motions of the diffusion MRI were corrected, and the individual skull-stripped T1-weighted images were transformed to the subjects' b0 images (non-diffusion-weighted image with $b = 0\ s/mm^2$). Next, the human and macaque T1 images were normalized to the standard structural ICBM152 and INIA19 templates for the humans and macaques, respectively. Finally, an inverse transformation was applied to the masks of the human and macaque bilateral PCuns in standard space to transform them into diffusion space for fiber tracking.

2.6. Resting-state fMRI data preprocessing

The in-house resting-state fMRI data were preprocessed using SPM8 software (http://www.fil.ion.ucl.ac.uk/spm). The preprocessing followed standard procedures, including discarding the first 10 vol to allow for MR equilibrium, slice timing, head motion correction by realigning to the first volume, normalizing to MNI space, smoothing using a Gaussian kernel of 6 mm full-width at half maximum (FWHM), and filtering with a temporal band-pass 0.01–0.1 Hz filter. Finally, the six motion parameters, white matter, cerebrospinal fluid, and global mean signals were regressed out. To control for the effects of head motion artefacts on the functional connectivity, the data were discarded if the head movement exceeded 2 mm translation or 2 degrees of rotation. Based on these criteria, none of the datasets in the present study were excluded.

2.7. Analyses I: anatomical connectivity- and coactivation-based parcellation of the human PCun

2.7.1. Definition of seed masks for the human PCun

The human PCun was defined based on the Desikan-Killiany (DK) atlas (Desikan et al., 2006). First, each individual PCun was extracted using Freesurfer (https://surfer.nmr.mgh.harvard.edu/) and transformed to 3D volume in Montreal Neurological Institute (MNI) space. Next, the PCun seed masks from all the subjects were used to create population-level probability maps (threshold >25% probability, binarized for the subsequent analysis). Finally, the resulting seed masks for the bilateral PCun subregions were transformed into individual diffusion space and were employed as seeds for both probabilistic fiber tracking and a connectivity-based parcellation analysis (Fan et al., 2016). In addition, the binarized seed masks of the PCun in MNI space were resampled to 2 mm cubic voxels for the coactivation-based parcellation (Wang et al., 2017d).

2.7.2. Probabilistic fiber tracking

Diffusion probabilistic tractography and voxel-wise probability distributions were estimated for two fiber directions using the FSL package (Behrens et al., 2007). Using the HCP data, for each voxel in the seed region, 5,000 streamlines were employed and the connectivity probability between each seed voxel and each voxel in the rest of the brain was estimated. The resulting anatomical connectivity matrix thus consisted of rows for each PCun voxel and columns for each voxel of the whole brain. Next, a symmetric cross-correlation matrix was generated by multiplying the connectivity matrix by its transposed matrix. The size of this cross-correlation matrix corresponds to the number of voxels in the PCun seed mask × the number of voxels in the PCun seed mask, and the *(i, j)th* element value is the correlation between the connectivity profile of seed voxel *i* and the connectivity profile of seed voxel *j* (Johansen-Berg et al., 2004).

2.7.3. Anatomical connectivity-based parcellation of the human PCun

In line with previous publications, a similarity matrix was segmented using spectral clustering to determine the different numbers of subregions clusters ranging from 2 to 7 (Fan et al., 2014; Wang et al., 2012, 2015a; Xu et al., 2015; Yang et al., 2016; Zhang et al., 2016). Next, maximum probability maps (MPM) were created for each solution across all subjects. To calculate the MPM, the subject-specific individual parcellation result was transformed from diffusion to MNI space. The maximum probability map, which used all the subjects' parcellation results in standard space, was calculated by assigning each voxel of the reference space to the area in which it was most likely to be located. If two areas showed the same probability at a particular voxel, this voxel was assigned to the area with the higher average probabilities of the 26 voxels directly adjacent (Eickhoff et al., 2005; Wang et al., 2012).

2.7.4. Coactivation-based parcellation

Task-related coactivation patterns have been increasingly employed to parcellate the functional architecture of the human brain. The task-related coactivation pattern was mapped on the basis of the meta-analytic connectivity modeling (MACM) approach (Eickhoff et al., 2012; Robinson et al., 2010), which identifies global coactivation patterns across several task paradigms. The theory behind MACM is that groups of coordinates that coactivate across experiments can be pooled to identify functionally connected networks in the brain (Robinson et al., 2010). Previous research indicated that coactivation-based parcellation approaches reveal highly concordant results about the functional architecture of the brain when compared with evaluated approaches, including cytoarchitectonic, anatomical, and resting-state functional connectivity-based mapping (Bzdok et al., 2013; Clos et al., 2013; Wang et al., 2015b, 2017d). Therefore, we implemented an additional coactivation-based parcellation approach to study the functional architecture of the PCun during task processing to reveal a consistent structural and functional topography of the PCun. To this end we initially mapped the whole brain coactivation pattern for each PCun voxel using the BrainMap database (Laird et al., 2009, 2011). The coactivation patterns were defined using this database of PET and fMRI experiments from healthy subjects and corresponding coordinates in stereotaxic space. The corresponding experiments derived from the BrainMap database included different functional domains ranging from perceptual to higher order cognitive functions, such as observation, vision motion, working memory, as well as social cognitive functions. To reliably define the task-dependent coactivation patterns of the voxels in the PCun, the voxels in the neighborhood of each seed voxel were pooled. Next, experiments reporting activations closest to the current seed voxel (extent of this spatial filter ranging from 20 to 200 experiments in steps of 5) were identified by calculating and subsequently sorting the Euclidian distances between a given seed voxel and any reported activation (Wang et al., 2015b, 2017d). Next, the whole brain coactivation pattern for each PCun voxel was calculated by means of an activation likelihood estimation (ALE) meta-analysis performed on the experiments associated with that particular voxel (Eickhoff et al., 2009, 2012; Turkeltaub et al., 2012). The ALE scores for each voxel in the gray matter were then recorded as the coactivation pattern for this voxel (Bzdok et al., 2013; Cieslik et al., 2013). The coactivation maps for all the seed voxels was subsequently combined into an N × M matrix where N was the number of seed voxels in the PCun and M was the number of target voxels throughout the whole brain. Finally, the parcellation of the PCun was performed with K = 2, 3 … 7 using one minus the correlation between the connectivity patterns of

the individual seed voxels as the correlation distance measure (Clos et al., 2013).

2.7.5. Determining the optimal number of subregions of the PCun

The Dice coefficient was used to evaluate the degree of overlap between the anatomical connectivity-based and coactivation-based parcellation results to identify corresponding structural and functional topographies for the PCun and, thus, to determine the optimal parcellation of subregions in the PCun (Dice, 1945; Wang et al., 2015b). The maximum Dice coefficient was considered to reflect the optimal PCun parcellation and was determined by computing the overlapped number of voxels between the maximum probability maps from the anatomical connectivity-based parcellation and the coactivation-based parcellation results.

2.7.6. Delineating the subregion-specific functional networks of the PCun

To map the subregion-specific intrinsic functional networks of the PCun subdivisions, a resting state functional connectivity approach was employed. To this end, we resampled each PCun subregion mask generated by overlapping the anatomical connectivity and coactivation pattern-based parcellation to 3 mm^3 voxels in MNI space. Next, a whole brain RSFC analysis using Pearson correlation coefficients between the mean time series for each subregion and each voxel at the whole-brain level was computed to determine subregion-specific networks, and the resulting FC maps were Fisher's z-transformed to improve normality. The resulting z-values maps were subsequently entered into a voxel-wise random effects one-sample *t*-test and thresholded at $p < 0.05$ (family wise error, FWE, corrected at the cluster level, initial cluster forming threshold, voxel-level $p < 0.001$ to identify the subregion-specific networks).

2.7.7. Whole brain coactivation patterns of each subregion

Structure-based meta-analysis and meta-analytical connectivity modeling (MACM) approaches, which pooled at least one focus of activation in the particular PCun subregion, were used to obtain the task-related coactivation patterns for each PCun subregion in the BrainMap database (Eickhoff et al., 2010; Laird et al., 2013; Robinson et al., 2010). Next, an ALE meta-analysis and the corresponding statistical inferences were performed to identify brain regions that coactivate with a specific PCun subregion. For the statistical inference, the ALE score was compared to a null-distribution reflecting a random spatial association between experiments with a fixed within-experiment distribution of foci (Eickhoff et al., 2009). This random-effects inference evaluates the above-chance convergence between experiments rather than the clustering of foci within a particular experiment. The ALE scores from the actual meta-analysis of the experiments activated within a particular subregion were then tested against the ALE scores obtained under this null-distribution, yielding a *p*-value based on the proportion of equal or higher random values (Eickhoff et al., 2012). These non-parametric *p*-values were then converted to z-scores and thresholded at $p < 0.05$ (cluster-level FWE-corrected, cluster-forming threshold at voxel-level $p < 0.001$) (Wang et al., 2017d).

2.7.8. Overlap and specific networks of each subregion

To identify common networks shared by the resting-state and coactivation patterns of each subregion, whole brain RSFC and coactivation networks for each subregion of the PCun were initially computed and thresholded at a FWE-corrected cluster-level threshold of $p < 0.05$ (details see above). Finally, subregion-specific conjunction analyses (i.e. the intersection connectivity analysis) were performed to determine convergent networks between the two approaches (coactivation and resting-state networks). In addition, we mapped the resting state functional connectivity and task-related coactivation patterns between the PCun subregions to determine subregion-specific networks of the PCun. Subregion-specific networks were defined as regions that showed significantly higher coupling with a given subregion in both resting-state functional connectivity and task-dependent coactivation patterns as compared to all other subregions.

2.7.9. Functional characterization of each subregion

The functional characterization of each PCun subregion was determined by employing behavioral domain and paradigm class analyses with the BrainMap database using forward inferences (Bzdok et al., 2013; Cieslik et al., 2013; Clos et al., 2013; Rottschy et al., 2013; Wang et al., 2015a, 2015b, 2016, 2017a, 2017b, 2017c) to identify the (sub-)domains that demonstrated a significantly higher probability of activation for a particular subregion (relative to the overall chance level). Statistical inference was based on nominal testing ($p < 0.05$ corrected for multiple comparisons by FDR) (Benjamini and Hochberg, 1995; Clos et al., 2013; Eickhoff et al., 2011).

2.8. Analyses II: comparisons of anatomical connectivity patterns of PCun subregions between humans and macaques

2.8.1. Human and macaque relative gray matter volume of precuneus

Voxel-based morphology (VBM) approach was used to calculate the gray matter volume in human and macaque with SPM8 package (http://www.fil.ion.ucl.ac.uk/spm) (Wang et al., 2017b; Wu et al., 2017). The human VBM analyses mainly included the following steps: 1), all the structural T1 images were segmented into gray matter, white matter, and cerebrospinal fluid; 2), the segmented images were registered to MNI space by applying high dimensional DARTEL normalization; 3), the normalized GM images were modulated to account for volume changes resulting from the normalization process. For the macaque brain, the details for calculating the gray matter volume have been described in our previous study (Wang et al., 2018). The main procedures for macaque VBM analysis included: 1), manually stripping the original structural T1 image of the skull for each subject and rotating the skull-stripped T1 image to match the orientation of the template image (the INIA19 template (Rohlfing et al., 2012) was used in this study); 2), each subject's T1 image was automatically segmented into gray matter, white matter and cerebrospinal fluid and was then transformed to the INIA19 template using DARTEL-normalization; 3), mean template images of gray matter, white matter, cerebrospinal fluid were created and each individual gray matter volume was transformed into the new mean gray matter template image. After obtained the segmented results in human and macaque, the total gray matter volume of precuneus and the whole brain in macaque data, HCP data, and in-house data were calculated. The absolute and relative gray matter volumes of precuneus defined as the total gray matter volume of precuneus divided by the total whole brain gray matter volume were computed. To determine the significant differences in absolute and relative gray matter volume, two-sample *t* tests were used and the significant level was set at $P < 0.05$ with Bonferroni correction.

2.8.2. Anatomical connectivity-based parcellation of macaque PCun

The macaque PCun subregions were defined using the macaque tractographic cortical atlas, which is based on an anatomical connectivity-based parcellation approach (for details see our previous paper presenting the atlas (Wang et al., 2018)). In our previous study, the macaque PCun seed masks were first defined using macroscopic landmarks (sulci or gyri) based on the NeuroMaps atlas (Rohlfing et al., 2012). Next, probabilistic fiber tracking was applied to obtain the whole brain anatomical connectivity pattern for each voxel in the PCun and spectral clustering was used to determine the subdivisions of the macaque PCun. Then, each individual parcellation result was transformed to template space and a maximum probability map for each solution was calculated. Finally, a continuity index was used to determine the optimal parcellation result for the macaque PCun, and a three-way parcellation scheme for the macaque PCun was obtained and used as a guide for further analyses. Thus, in the present study, the anatomical connectivity profiles of the 3 subregions of the macaque PCun were mapped and compared to the human PCun subregions.

2.8.3. Whole brain anatomical connectivity patterns in humans and macaques

To examine whether the PCun subregions in humans and macaques share anatomical connectivity patterns, whole brain anatomical connectivity patterns for each PCun subregion were mapped in humans and macaques. To this end seed masks of the PCun subregions were transformed to diffusion space and Probtracking was used to obtain connectivity probabilities between each PCun subregion and all other voxels in the brain (Behrens et al., 2003). 5,000 samples were generated from the connectivity distribution for each voxel and the connection probability for each voxel was calculated. Finally, the identified fiber tracts were converted to standard space and averaged across the connection probability maps to obtain PCun subregion-specific mean probability connectivity maps for both humans and macaques.

2.9. Between-species comparison of specific anatomical pathways

2.9.1. Definition of target brain areas

The target brain areas were defined based on previous findings reporting homologous and similar connectivity patterns of the PCun in both humans and macaques (Cavanna and Trimble, 2006; Leichnetz, 2001; Margulies et al., 2009; Markov et al., 2011). Based on these findings, 17 homologous target brain areas in humans and macaques, which had been identified in previous anatomical and functional studies, were defined: the anterior cingulate cortex (ACC) (Neubert et al., 2015; Touroutoglou et al., 2016), basal ganglia areas including the caudate (CAU), putamen (PUT), and thalamus (THA) (Croxson et al., 2005; Draganski et al., 2008; Haber and Knutson, 2010), cuneus (CUNE) (Catani et al., 2003; Hutchison et al., 2015; Morecraft et al., 2004), inferior frontal gyrus (IFG) (Croxson et al., 2005; Nakahara et al., 2002; Neubert et al., 2014), superior and middle frontal gyrus (SFG/MFG) (Croxson et al., 2005; Sallet et al., 2013), dorsal premotor cortex (PMd) (Geyer et al., 2000; Passingham et al., 1998; Picard and Strick, 2001; Tomassini et al., 2007), supplementary motor area (SMA) (Johansen-Berg et al., 2004; Morecraft et al., 2012; Sallet et al., 2013), supramarginal gyrus (SMG) (Caspers et al., 2011; Mars et al., 2011; Pandya and Seltzer, 1982), hippocampus and parahippocampus (HIPP/ParaHIPP) (Blatt et al., 2003; Rosene and Van Hoesen, 1977; Saunders and Rosene, 1988; Saunders et al., 1988; Squire, 1992; Suzuki and Amaral, 1994; Vincent et al., 2010), insula (IN) (Deen et al., 2011; Mesulam and Mufson, 1982; Mufson and Mesulam, 1982), and three temporal areas including the superior, middle, and inferior temporal gyri (STG/MTG/ITG) (Borra and Luppino, 2017; Gil-da-Costa et al., 2006; Hackett et al., 2001; Tsao et al., 2008). Although whether middle temporal gyrus in human and macaque is homogenous remains an open problem, given that both tract-tracing and functional connectivity analyses identified interconnection between PCun and posterior middle temporal gyrus (Margulies et al., 2009; Parvizi et al., 2006) and comparison mapping also identified functional homogeneity of temporoparietal junction between human and macaque (Mars et al., 2013), we thus included MTG in our study to map the anatomical connectivity pattern for each PCun subregion. The target brain areas in humans were defined based on structural maps from the automatic anatomical labeling (AAL) atlas and the dorsolateral frontal cortex tractographic atlas yielded by anatomical connectivity-based parcellation (Sallet et al., 2013). Corresponding target areas for the macaques were extracted from the NeuroMaps atlas and a recently published MRI macaque atlas incorporating 241 brain areas developed using high-resolution MRI data (Calabrese et al., 2015). For fiber tracking, the PCun subregions and target masks were transformed to individual diffusion space.

2.9.2. Anatomical connectivity mapping

Probabilistic fiber tracking with 5,000 streamlines from each voxel in the PCun subregions was performed to map the anatomical connectivity between the PCun subregions and target brain areas using FSL. To control for inter-individual variability, the tracking results were initially normalized using a log transformation and by dividing each voxel's value by the maximum voxel value in the respective map (values between 0 and 1) (Mars et al., 2016). Finally, the anatomical connectivity probabilities for each PCun subregion and each target were determined.

2.9.3. Comparisons of anatomical connectivity patterns

To further evaluate the anatomical connectivity fingerprints between the humans and macaques, the anatomical connectivity fingerprints of each subregion were further normalized across all the targets, such that the maximum connectivity probability between a precuneus subregion and any of the target brain areas had a value of 1 and the minimum connectivity probability had a value of 0 using the following formula.

$$p_{i,j} = \frac{p_{i,j} - \min\ (p_i)}{\max\ (p_i) - \min\ (p_i)}$$

Where $p_{i,\,j}$ is the connectivity probability between the *i*th precuneus subregion and the *j*th target brain area. The max (p_i) is the maximum connectivity probability between the *i*th precuneus subregion and all the target brain areas, whereas the min (p_i) is the minimum connectivity probability between the *i*th precuneus subregion and all the target brain areas. The normalized anatomical connectivity probability values were used to construct the anatomical fingerprints for each precuneus subregion. Finally, to quantitatively characterize the similarity between humans and macaques, the Manhattan or city-block distance index was calculated between the fingerprints of the humans and macaques (Sallet et al., 2013).

2.10. Reproducibility and cross-validation analyses

To determine the robustness of the concordance between the anatomical- and coactivation-based parcellations, identical analysis were performed on an independent in-house dataset to parcellate the human PCun into 2 to 7 subregions based on distinct whole brain anatomical connectivity patterns. The maximum probability map was created in MNI space and overlapped with the coactivation-based parcellation results at each solution to determine whether the concordant topography identified in the HCP data was reproducible. In addition, the Dice coefficient was used to quantitatively measure the overlap degree between the two concordant topographies obtained separately from the HCP and in-house datasets.

In addition, the whole brain anatomical connectivity patterns and target-based anatomical connectivity fingerprint for each PCun subregion was mapped with the in-house diffusion data using identical procedures for cross-validation.

3. Results

3.1. Analyses I: anatomical connectivity- and coactivation-based parcellations of the human PCun

3.1.1. Convergent anatomical and coactivation topography of the human PCun

The degree of overlap between the MPMs obtained from anatomical connectivity- and coactivation-based parcellations yielded an optimal parcellation of the PCun into 3 subregions in both sets of data (HCP and in-house) (Figs. 1 and 2A). Cross-validating the results between the datasets revealed a high degree of overlap (left PCun, 0.935; right PCun, 0.929) (Fig. 2B); consequently, the 3 subregion parcellation was used in the subsequent analyses.

More specifically, the parcellation revealed (1) a posterior dorsal PCun subregion located anterior to the parieto-occipital sulcus (cluster 1; red/label L1, R1; MNI center coordinate: L1, [-16 -68 28]; R1, [13–69 28]), resembling the cytoarchitectonically defined area 7M (Fig. 2); (2) an anterior dorsal PCun subregion located posterior to the marginal branch of the cingulate sulcus (cluster 3, yellow/label L3, R3; MNI center

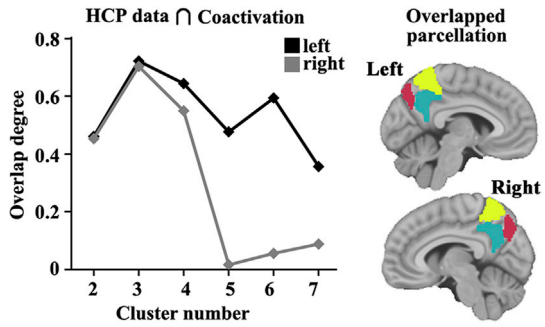

Fig. 1. Anatomical connectivity and coactivation-based parcellation of the human precuneus (PCun) using Human Connectome Project (HCP) data. The overlap degree between the maximum probability map (MPM) of the PCun yielded by anatomical connectivity-based parcellation using HCP data and the parcellation results for the PCun obtained by coactivation-based parcellation were calculated for each solution (K = 2 … 7). The maximum overlap degree between the anatomical connectivity and coactivation-based parcellation results was used to determine the optimal parcellation scheme for the left and right PCun. In the end, a three-way parcellation scheme of the left and right PCun was found and used to guide the further analyses.

coordinate: L3, [-7 -51 56]; R3, [7–52 57]), resembling the cytoarchitectonically defined area 5M (Fig. 2); and (3) a ventral PCun subregion located dorsal to the posterior cingulate cortex (cluster 2, navy blue/label L2, R2; MNI center coordinate: L2, [-6 -55 33]; R2, [6–55 32]), corresponding to the cytoarchitectonically defined Brodman area (BA) 31 (Figs. 1 and 2). Recently, Glasser et al. (2016) built a cerebral cortical atlas using multi-modal neuroimaging technique, and seven different subregions in the corresponding precuneus were identified. Compared to the cortical atlas, the posterior dorsal PCun subregions (L1/R1) corresponded to the areas of POS2 and DVT; the anterior dorsal PCun subregions (L3/R3) were similar to the areas of 7Am, 5mv, and PCV; and the

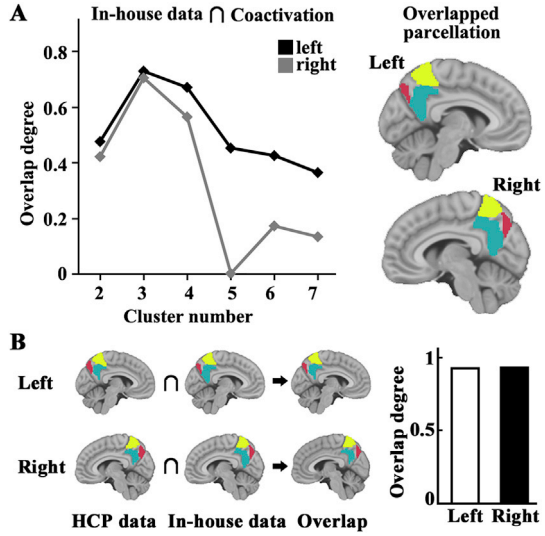

Fig. 2. Cross-validation analyses of the consistent topography of the precuneus (PCun) from anatomical connectivity and coactivation-based parcellation in an independent in-house dataset. A. The overlap degree between the maximum probability map (MPM) of the PCun yielded by anatomical connectivity-based parcellation using in-house data and the parcellation results of the PCun obtained by coactivation-based parcellation was calculated for each solution (K = 2 … 7). The optimal three-way parcellation scheme of the PCun was also identified using in-house data. B, The overlap degree between the consistent topographies of the PCun obtained using Human Connectome Project (HCP) data and in-house data was calculated. The overlap degree showed high consistency of the parcellation results for the PCun in the two sets of data (left PCun, 0.935; right PCun, 0.929).

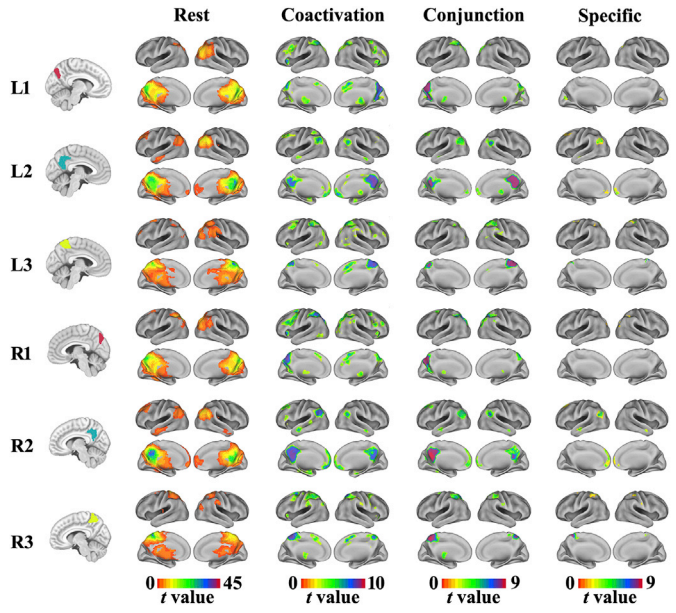

Fig. 3. Whole brain resting-state functional (RSFC), coactivation, conjunction, and specific connectivity patterns for each precuneal (PCun) subregion. The first column is the anatomical location for each PCun shown on a structural template. The second column is the whole brain RSFC patterns for each cluster obtained using one sample *t*-tests (thresholded at $p < 0.05$, cluster-level FWE-corrected, cluster-forming threshold at voxel-level $p < 0.001$). The third column is the whole brain coactivation connectivity pattern for each subregion of the PCun obtained using meta-analytical connectivity modeling (MACM) (thresholded at $p < 0.05$, cluster-level FWE-corrected, cluster-forming threshold at voxel-level $p < 0.001$). The forth column is the overlapping connectivities between the RSFC and coactivation patterns for each PCun subregion. The last column is the specific resting-state and coactivation connectivity pattern for each PCun cluster.

ventral subregions (L2/R2) resembled the areas 7 m, 31a, v32ab, 31pd and 31pv.

3.1.2. Resting-state functional network of the PCun subregions

Findings from the subregion-specific whole brain resting-state functional connectivity networks are presented in Fig. 3. L1 and R1 showed predominantly functional connectivity with the CUNE, inferior parietal lobule (IPL), ParaHIPP, and THA, and R1 additionally connected to the left frontal eye field (FEF). The ventral subregions, L2 and R2, showed the strongest connections with the dorsolateral prefrontal cortex (dlPFC), bilateral angular gyrus (AG), medial prefrontal cortex (MPFC), ParaHIPP, and THA. L3 and R3 demonstrated strong connectivity with the occipital cortex, intraparietal sulcus (IPS), FEF, middle cingulate cortex, striatum, THA, and SMG. R3 additionally displayed connections with the right FEF and left posterior IN, whereas L3 was additionally related to the frontal pole (FP).

3.1.3. Coactivation network of each subregion

Using MACM to map whole brain coactivation connectivity patterns yielded similar networks, resembling the findings from the resting-state functional connectivity approach (Fig. 3). Moreover, the coactivation approach additionally revealed that L1 and R1coactivated with the bilateral inferior frontal sulcus (IFS), SMA, anterior IN, and right anterior MFG; L2 coactivated with the anterior cingulate cortex; and L3 and R3 additionally coactivated with the lateral occipital gyrus, SMA, anterior IN, MFG, and IFG.

3.1.4. Corresponding resting state and task coactivation networks for each subregion

The intersection between the resting-state and coactivation

connectivities was calculated to obtain the corresponding connectivity patterns for each subregion at rest and during a task (Fig. 3). Conjunct connectivities for L1 and R1 were found in the CUNE, IPS, and THA, and R1 was additionally connected to the left FEF. For L2 and R2, the conjunct connections were primarily observed in the dlPFC, AG, MPFC, and ParaHIPP. Conjunctions between the resting-state and coactivation for the L3 and R3 were found in the IPS, SMG, and FEF. The L3 had additional conjunct connectivity with the anterior cingulate cortex, whereas the R3 had additional conjunct connectivity with the THA.

3.1.5. Subregion-specific network determination of the PCun

Determining the subregion-specific PCun networks across the approaches (Fig. 3) demonstrated that L1 and R1 had a specific relationship to the CUNE; L2 and R2 had specific relationships with the AG, dlPFC, MPFC, and ParaHIPP; L3 and R3 had specific relationships with the IPS and FEF; and R3 was specifically connected to the SMG.

3.1.6. Functional characterization of each subregion

Mapping the primary functional contributions of the subregions revealed that L1 was primarily associated with explicit memory and reasoning and R1 was primarily associated with visual motion processing, spatial cognition, working and explicit memory. Both L2 and R2 were significantly associated with social cognition and explicit memory. L2 was additionally associated with reasoning and emotion, whereas R2 was additionally associated with language processing. Significant associations were found for L3 with somatic processing, spatial cognition, visual motion processing and working memory. For R3, the main functions were imagination, spatial cognition, and observation (Fig. 4).

3.2. Analyses II: comparisons of anatomical connectivity patterns of PCun subregions between humans and macaques

3.2.1. Human and macaque PCun relative gray matter volume comparisons

The macaque and human structural T1 images were segmented into gray matter, white matter, and cerebrospinal fluid in all the datasets (Fig. 5A), and the significant differences in absolute and relative gray matter volume of precuneus between human and macaque were found (all $P \approx 0$) (Fig. 5B and C). The relative gray matter volume of the human precuneus was about 1/50 of the total brain gray matter volume in both HCP data and in-house data. In macaque, the relative gray matter volume of the precuneus was about 1/100. Generally, the relative gray matter volume of precuneus in human is about two-fold higher than that in macaque.

3.2.2. Macaque PCun subregions and defined target brain areas

The macaque PCun subregions were defined based on our previously published macaque cortical atlas (Wang et al., 2018). In the current study using an anatomical connectivity-based parcellation approach, the

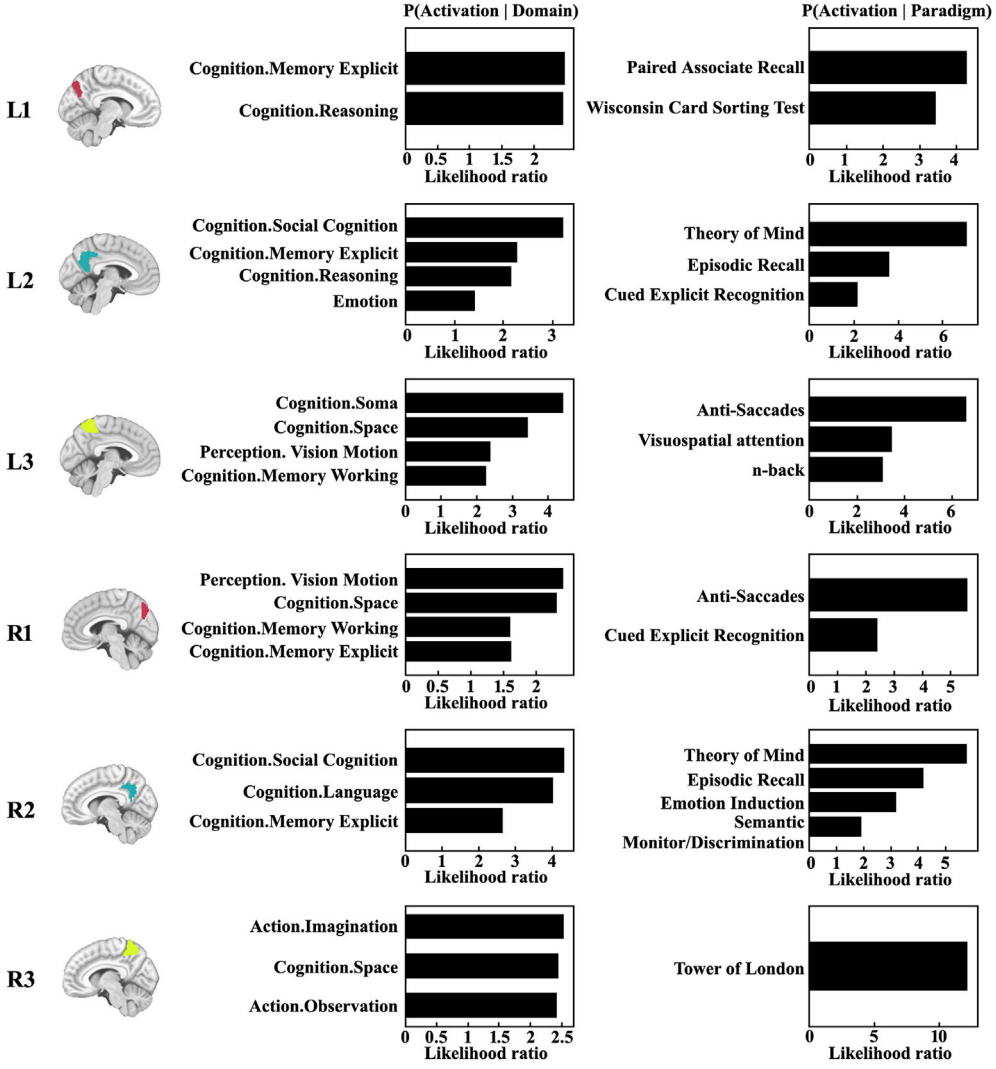

Fig. 4. Functional characterization of each precuneal (PCun) subregion. Forward inference was used to determine the functional organization of each PCun subregion. The significant activation probabilities for each subregion with respect to a given domain or paradigm in a cluster are depicted separately.

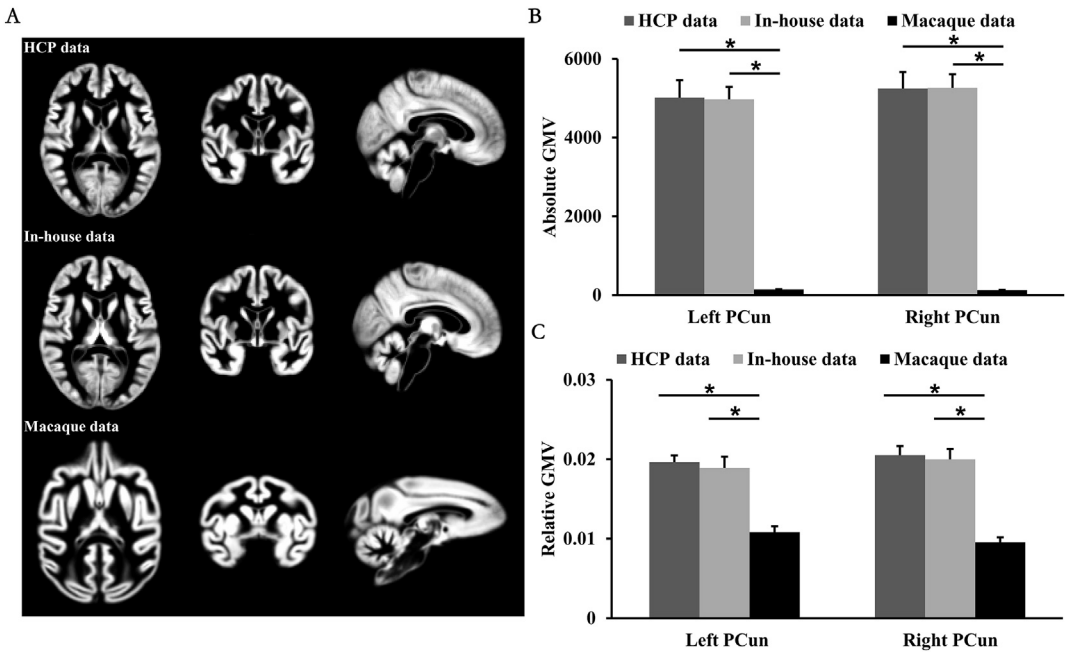

Fig. 5. Human and macaque precuneus absolute and relative gray matter volume. A. human and macaque structural T1 images were segmented into gray matter, white matter, and cerebrospinal fluid and the gray matter segmentation results were shown. B. The absolute gray matter volume of precuneus in human and macaque were calculated and the compared. Significantly larger absolute gray matter volume of precuneus was found in human compared to macaque. C. The relative gray matter volume of precuneus in human and macaque were calculated and the compared. Significantly greater relative gray matter volume (about two-fold) of precuneus was found in human compared to macaque. * represents the significant differences.

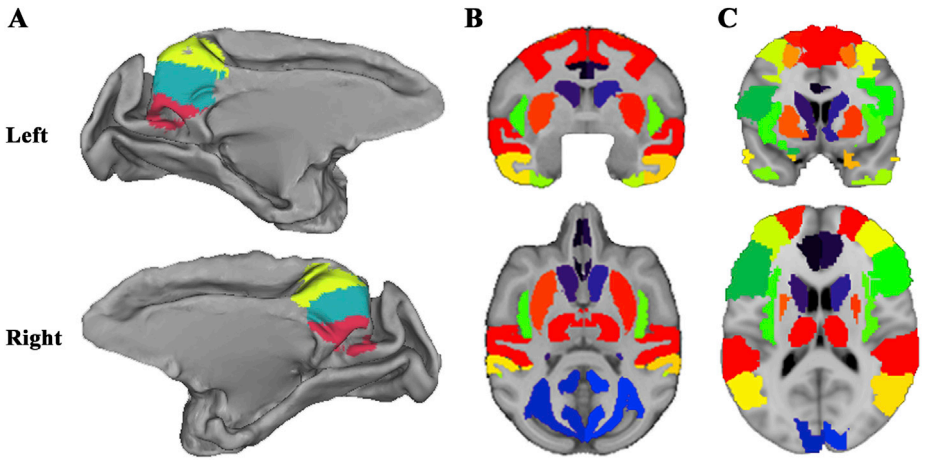

Fig. 6. Macaque precuneal (PCun) parcellation results and homologous target brain areas in humans and macaques. A. Macaque PCun was parcellated into three subregions using an anatomical connectivity-based parcellation approach in our previous study. B. 17 target brain areas in the macaque brain were defined and used to map the anatomical connectivity fingerprint. C. 17 homologous target brain areas in the human brain were also defined and used to map the anatomical connectivity fingerprint.

macaque PCun was parcellated into three subregions (Fig. 6A). Then, each PCun subregion was extracted and used as a seed mask to map the anatomical connectivity patterns. To map the anatomical connectivity fingerprints for the PCun subregions, we defined 17 homologous target brain areas that showed connections with PCun in both humans and macaques. The target brain areas were the ACC, CAU, CUNE, HIPP, IFG, INA, ITG, MFG, MTG, ParaHIPP, PMd, PUT, SFG, SMA, SMG, STG, and THA (Fig. 6B and C).

3.2.3. *Whole brain anatomical connectivity*

The whole brain anatomical connectivity pattern of each PCun subregion was mapped in humans and macaques using probabilistic tracking. The whole brain anatomical connectivity maps for the PCun were highly consistent between humans and macaques (Fig. 7). For L1 and R1 the main anatomical connections were found in the occipital cortex, striatum, THA, ParaHIPP, ITG, superior temporal sulcus, and frontal cortex via the inferior longitudinal fasciculus (ILF), corticospinal tract (CST) and corpus callosum (CC). The structural connectivities of L2 and R2 were primarily to the cingulate, dorsomedial prefrontal cortex, MPFC, striatum, THA, INA and ITG through the ILF, CC, CST, and cingulate bundle. L3 and R3 primarily connected with the striatum, THA, cingulate cortex, SMA, STG, INA, and FEF through the CC, cingulate bundle, superior longitudinal fasciculus (SLF), CST and extreme capsule (EmC). The presence of similar whole brain anatomical connectivity patterns between human and macaque PCun subregions were validated using an independent in-house dataset (Fig. S1).

3.2.4. *Comparisons of anatomical connectivity patterns*

The anatomical connectivity fingerprints further demonstrated that PCun subregions shared similar anatomical connectivity patterns in macaques and humans (Fig. 8), which was further confirmed using the in-house dataset (Fig. S2). By quantitatively characterizing the connectivity

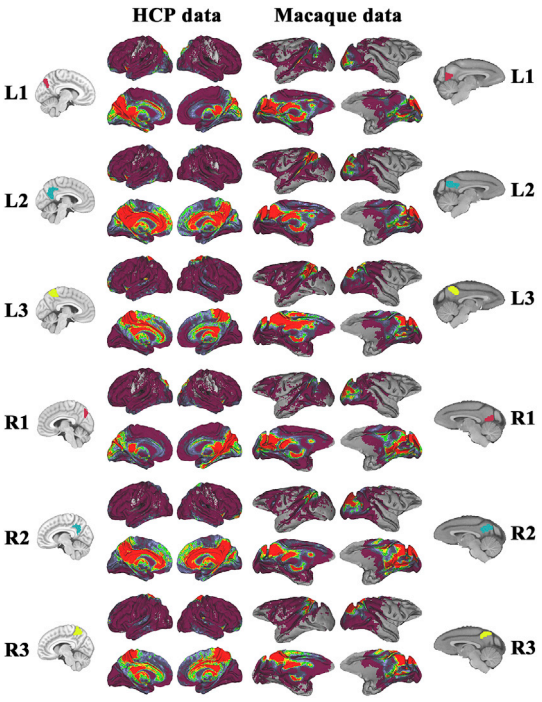

Fig. 7. Whole brain anatomical connectivity patterns for each subregion of the precuneus (PCun). Whole brain population maps of the probabilistic tractography results for each subregion of the PCun were mapped. In the human brain, the whole brain anatomical connectivity patters for the PCun were mapped using Human Connectome Project (HCP) data. The whole brain anatomical connectivity map for each PCun subregion showed similar connectivity patterns in humans and macaques.

similarity, we found that L1 and R1 showed high anatomical connectivity probability with CAU, INA, SMA, SMG, and THA in both humans and macaques. For the L3 and R3, the main anatomical connections were found in the CUNE, PUT, and THA in both humans and macaques. The ventral L2 and R2 primarily connected to CAU, CUNE, PUT, SMG, and THA. The target-based connectivity fingerprint for each PCun subregion was similar to the whole brain anatomical connectivity maps for each subregion. The comparison of the PCun subregions' anatomical connectivity patterns between humans and macaques revealed that the human L1/R1, L2/R2, and L3/R3 corresponded to the macaque L1/R1, L2/R2, and L3/R3 subregions, respectively.

4. Discussion

Using anatomical connectivity and task-dependent coactivation patterns, our present study identified a convergent functional topography of the human PCun and suggested that anatomical connectivity can reflect the task-related functional architecture. Furthermore, a macaque dataset demonstrated similar anatomical connectivity patterns of the PCun subregions across the species, suggesting that the PCun may have evolved similar functional roles in humans and macaques.

Combining anatomical connectivity and task-related coactivation approaches allowed us to determine a convergent topographical organization of the PCun that includes two subregions in the dorsal PCun and one in the ventral PCun. The identified topological organization is in accord with previous findings based on microscopic cytoarchitecture and myeloarchitecture as well as macroscopic neuroimaging approaches. Moreover, the present study found highly overlapping PCun networks across anatomical, resting-state, and task-related coactivation networks. The relationship between structure and function has been addressed in several previous studies with some reporting that the functional connectivity was structured by the anatomical connectivity (Damoiseaux and Greicius, 2009; Deco et al., 2013; Wang et al., 2015b, 2016); however, other studies reported that functional connectivity was present in the absence of anatomical connectivity (Damoiseaux and Greicius, 2009; Zhang et al., 2010). Furthermore, the quantitative analyses comparing the structural and functional connections identified a high correlation between the two types of connectivities (Honey et al., 2009). In general, the integrative analysis approach identified highly correspondent architectures for a number of brain areas across different types of connectivity profiles. The application of integrative approaches can provide a more reproducible and reliable methodological strategy for identifying relationships between structural and functional networks relationship than quantitative analysis.

Three subregions in the PCun were identified using both anatomical connectivity and task-related coactivation patterns. The bilateral dorsal-posterior PCun (L1 and R1) subregions were specifically connected with the cuneus. Previous functional neuroimaging studies revealed that these

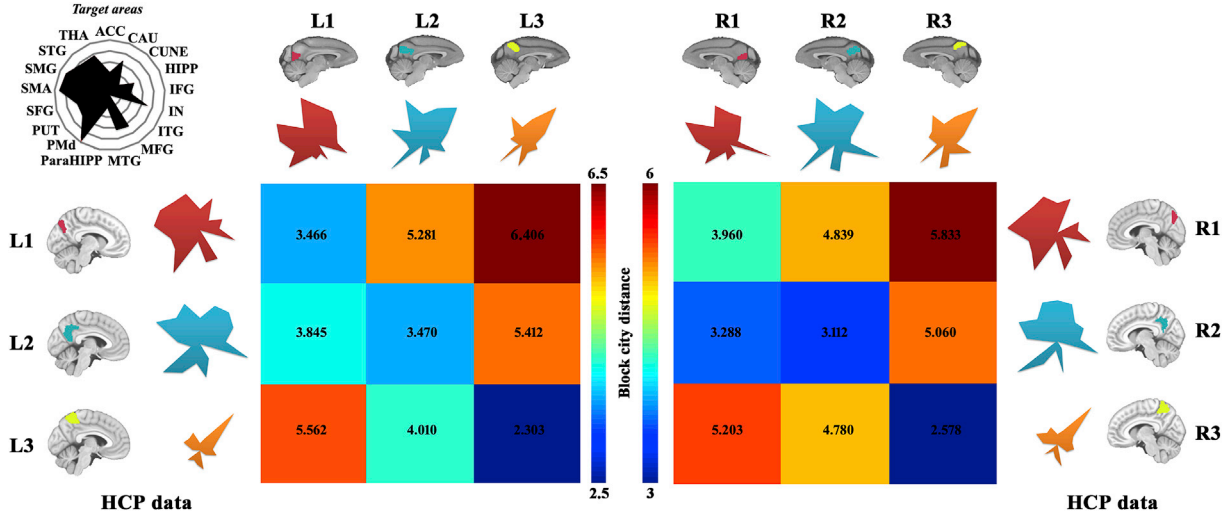

Fig. 8. Human and macaque anatomical connectivity fingerprints for each precuneal (PCun) subregion were mapped using Human Connectome Project (HCP) data and macaque diffusion MRI data. The anatomical connectivity probability between each PCun seed region and each target was obtained for humans and macaques. Then, the anatomical connectivity was normalized and the mean connectivity probability was used to map the anatomical connectivity fingerprints. The block-city distance was used to calculate the similarity between the fingerprints of each PCun subregion in humans and macaques. Anatomical connectivity fingerprints identified correspondent PCun subregions in humans and macaques.

two subregions were primarily involved in visual-spatial information processing (Hanakawa et al., 2003; Knauff et al., 2003; Leichnetz, 2001; Suchan et al., 2002). In addition, the functional characterization of the two subregions in our study found that the bilateral dorsal-posterior PCun subregion participates in working and explicit memory as well as in reasoning. Thus, these findings suggest that the dorsal-posterior PCun may play an important role in spatial working and explicit memory and in space-related reasoning (Knauff et al., 2003; Owen et al., 2005). The dorsal-anterior subregions of the PCun (L3 and R3) specifically connected with the frontal eye field (FEF) and ventral postcentral gyrus. The functionally connected areas also showed direct white matter anatomical connectivities (Szczepanski et al., 2013; Wu et al., 2016a). The specific connections of the dorsal-anterior PCun suggested that this area is closely related to spatially guided behaviors (Astafiev et al., 2003; Wenderoth et al., 2005). The functional characterization found that this area was also involved in action and attention processing, indicating that the dorsal-anterior PCun plays an important role in attentive tracking and attention shifting (Cavanna and Trimble, 2006; Culham et al., 1998; Simon et al., 2002). The ventral PCun specifically connected to default mode network-(DMN) related brain areas, including the medial prefrontal cortex (MPFC), inferior parietal lobule (IPL), and medial temporal lobe (MTL) (Greicius et al., 2003; Raichle et al., 2001). Our findings were consistent with previous functional connectivity analyses of this area (Cauda et al., 2010; Zhang and Li, 2012). The main functions associated with this area are social cognition and self-reference processing, and functional abnormalities of this area can serve as a biomarker to distinguish mild from severe Alzheimer's disease (AD) (Wu et al., 2016b). Functional characterization of this area in our study revealed that this area also participates in explicit memory, emotion, and language processing, findings which suggested that the ventral PCun plays a crucial role in functional integration and is the core brain area of the DMN (Hagmann et al., 2008). The functional differences suggested that the ventral PCun coordinates emotion, semantic, and episodic memory processing. However, whether the PCun belongs to the DMN is still controversial. Recent studies found that the posterior cingulate cortex (PCC) not the PCun belongs to DMN included (Buckner et al., 2008; Margulies et al., 2009). Given the close anatomical location of the ventral PCun and the PCC as well as the smoothing that occurs during functional preprocessing, the question of whether the ventral PCun belongs to the DMN needs to be investigated further.

Three subregions in macaque PCun were also identified. Our parcellation scheme for macaque PCun was supported by previous histological and functional mapping for this area. Using a combination of histological criteria and atlas-based landmarks, Markov et al. (2011) constructed a macaque cortical atlas called M132 and defined three subregions in PCun. Compared to the M132 atlas, the dorsal PCun subregion is similar to the medial area 5; the middle PCun subregion corresponded to the area of 7m; and the ventral PCun subregion resembled the area V6A. Using awake and anesthetized macaque fMRI data, Xu et al. (2018) recently performed the whole brain cortical parcellation of macaque and also identified three subregions in PCun, and the spatial arrangement showed a similar pattern from dorsal to ventral direction compared with our anatomical connectivity-based parcellation of this area. The similar topography of PCun further demonstrated that the brain functional topography was structured by its anatomical connectivity patterns (Wang et al., 2015b; Wang et al., 2016). The similar functional and anatomical connectivity based parcellation results for macaque PCun was consistent with the current finding that PCun has similar anatomical and task-related functional topography in human brain. Moreover, in the study of Xu et al (2018), a similar functional topographies during awake and anesthesia in macaque were found suggesting that the functional mapping can reveal the intrinsic functional organization of the macaque brain in spite of different physiological states. However, given that the functional signals are fast changes with time in human even during several munities' resting-state scanning (Allen et al., 2014), whether the whole brain functional topography are still stable with dynamic functional connectivity mapping needs to be further test.

Graph theory analyses have revealed that the PCun is the core network hub in the human brain (Gong et al., 2009; Hagmann et al., 2008). Recent tract-tracing and white matter anatomical network studies in macaques also revealed that the macaque PCun is a dominant hub area (Markov et al., 2011), possibly indicating that the PCun serves a similar integrative role in both humans and macaques. A recent resting-state functional connectivity analysis of the posteromedial cortex also identified convergent functional networks in humans and macaques (Margulies et al., 2009). Tract-tracking revealed that the dorsal-anterior PCun in macaques primarily connected with the superior parietal cortex and the supplementary motor and cingulate motor areas. The dorsal-posterior PCun primarily connected with the parieto-occipital fissure and cuneus. Also, the ventral PCun has strong connections with the dorsolateral prefrontal cortex, inferior parietal lobule, and the superior temporal sulcus (Parvizi et al., 2006). The tract-tracing findings in macaques were consistent with our tractographic results for the PCun subregions using diffusion MRI. In addition, the PCun anatomical connectivity patterns identified using tract-tracing in macaques were similar to the functional and anatomical connectivity analyses of the human PCun subregions (Cauda et al., 2010; Zhang and Li, 2012; Zhang et al., 2014). However, a recent comparative neuroanatomical study found a longitudinal, spatial dilation of the upper part of the PCun in humans relative to chimpanzees, so the authors concluded that precuneal expansion is a specialization of *Homo sapiens* and may be associated with human cognitive specializations (Bruner et al., 2017). Although Brunauer and colleagues found a great expansion of the PCun in humans (Bruner et al., 2017), whether the relative volume of the human precuneus is greater than that of chimpanzees or macaques is unknown. Therefore, the relationship between the expanded volume and functional specializations needs further study. Hill and colleagues reported high cortical expansion regions primarily located in lateral temporal, lateral parietal, and dorsal and medial prefrontal regions during evolution, but the medial parietal area expansion is much lower than these areas (Hill et al., 2010). Recently, Donahue et al. (2018) found that the absolute cortical gray matter volume of prefrontal cortex and its associated absolute white matter volume greatly expanded in human compared with macaque. However, the quantitative expansion of PCun in human compared to macaque is unclear. To address this question, we measured the relative gray matter volume of PCun in human and macaque and found that the relative gray matter volume in human was almost two-fold larger than that in macaque. Our finding was consistent with a previous report about the gray matter variability in human and macaque (Croxson et al., 2018). Taken together, the anatomical connectivity analyses of the PCun subregions, together with the previous tract-tracing and resting-state functional studies, strongly suggested that the PCun shares similar connectivity patterns in humans and macaques. These findings collectively demonstrated that the precuneus shows functional homology in humans and macaques.

In this study, the volumetric precuneus masks were defined for parcellation. The superiority of volume- or surface-based analyses has been widely discussed in this area. Recently, Coalson et al. (2018) addressed this issue emphasizing more accurate cortical areal localization using surface-based analysis than volume-based analysis. In fact, both approaches have advantages and disadvantages. The surface-based analysis has higher registration accuracy across subjects, more sensitive to detect the activation, and better to extract finer functional structures than volume analysis (Anticevic et al., 2008; Argall et al., 2006; Desai et al., 2005). The primary limitations of the surface based analysis are missing the subcortical information and requiring accurate projection from fMRI to structure MRI (Tucholka et al., 2012). The accurate projection, in view of the typical resolution of fMRI data, from functional data onto the cortical surface is a real challenge in practice due to small cortical thickness, small distance between the width of a gyrus or the banks of a given sulci, and the artefacts due to geometric distortions that are not systematically and fully corrected during pre-processing (Hutton et al.,

2002; Operto et al., 2008; Tucholka et al., 2012). Moreover, Tucholka et al. (2012) reported the incorrect projection of a computation task for surface-based analysis. Given these problems and to keep the rich cortical-subcortical-cerebellum connections of precuneus (Cavanna and Trimble, 2006; Zhang and Li, 2012), we adopted the volume-based analysis approach in this study.

In summary, we revealed a corresponding structural and task-dependent functional architecture of the PCun in the human brain using a connectivity-based parcellation approach. The parcellation scheme for the PCun was further supported by utilizing specific connectivity pattern mapping analyses and functional characterization. In addition, we identified shared functional PCun topographies and structural connectivity patterns in humans and macaques, suggesting that the PCun has evolved similar roles across species. Our findings provide more detailed information about the functional organization of the PCun and may facilitate future clinical, cognitive, and evolutionary research studies of this area.

Acknowledgments

This work was supported by the Natural Science Foundation of China (91432302, 31620103905), the Science Frontier Program of the Chinese Academy of Sciences (Grant No. QYZDJ-SSW-SMC019), National Key R&D Program of China (Grant No. 2017YFA0105203), Beijing Municipal Science and Technology Commission (Grant Nos. Z161100000216152, Z161100000216139), and the Guangdong Pearl River Talents Plan (2016ZT06S220). The authors thank Rhoda E. and Edmund F. Perozzi for editing assistance.

Appendix A. Supplementary data

Supplementary data to this article can be found online at https://doi.org/10.1016/j.neuroimage.2019.07.001.

References

Allen, E.A., Damaraju, E., Plis, S.M., Erhardt, E.B., Eichele, T., Calhoun, V.D., 2014. Tracking whole-brain connectivity dynamics in the resting state. Cerebr. Cortex 24, 663–676.

Anticevic, A., Dierker, D.L., Gillespie, S.K., Repovs, G., Csernansky, J.G., Van Essen, D.C., Barch, D.M., 2008. Comparing surface-based and volume-based analyses of functional neuroimaging data in patients with schizophrenia. Neuroimage 41, 835–848.

Argall, B.D., Saad, Z.S., Beauchamp, M.S., 2006. Simplified intersubject averaging on the cortical surface using SUMA. Hum. Brain Mapp. 27, 14–27.

Astafiev, S.V., Shulman, G.L., Stanley, C.M., Snyder, A.Z., Van Essen, D.C., Corbetta, M., 2003. Functional organization of human intraparietal and frontal cortex for attending, looking, and pointing. J. Neurosci. 23, 4689–4699.

Battaglia-Mayer, A., Caminiti, R., 2002. Optic ataxia as a result of the breakdown of the global tuning fields of parietal neurones. Brain 125, 225–237.

Behrens, T.E., Berg, H.J., Jbabdi, S., Rushworth, M.F., Woolrich, M.W., 2007. Probabilistic diffusion tractography with multiple fibre orientations: what can we gain? Neuroimage 34, 144–155.

Behrens, T.E., Johansen-Berg, H., Woolrich, M.W., Smith, S.M., Wheeler-Kingshott, C.A., Boulby, P.A., Barker, G.J., Sillery, E.L., Sheehan, K., Ciccarelli, O., Thompson, A.J., Brady, J.M., Matthews, P.M., 2003. Non-invasive mapping of connections between human thalamus and cortex using diffusion imaging. Nat. Neurosci. 6, 750–757.

Benjamini, Y., Hochberg, Y., 1995. Controlling the false discovery rate: a practical and powerful approach to multiple testing. J. R. Stat. Soc. Ser. B 57, 289–300.

Blatt, G.J., Pandya, D.N., Rosene, D.L., 2003. Parcellation of cortical afferents to three distinct sectors in the parahippocampal gyrus of the rhesus monkey: an anatomical and neurophysiological study. J. Comp. Neurol. 466, 161–179.

Borra, E., Luppino, G., 2017. Functional anatomy of the macaque temporo-parieto-frontal connectivity. Cortex 97, 306–326.

Bruner, E., Preuss, T.M., Chen, X., Rilling, J.K., 2017. Evidence for expansion of the precuneus in human evolution. Brain Struct. Funct. 222, 1053–1060.

Buckner, R.L., Andrews-Hanna, J.R., Schacter, D.L., 2008. The brain's default network: anatomy, function, and relevance to disease. Ann. N. Y. Acad. Sci. 1124, 1–38.

Bzdok, D., Laird, A.R., Zilles, K., Fox, P.T., Eickhoff, S.B., 2013. An investigation of the structural, connectional, and functional subspecialization in the human amygdala. Hum. Brain Mapp. 34, 3247–3266.

Calabrese, E., Badea, A., Coe, C.L., Lubach, G.R., Shi, Y., Styner, M.A., Johnson, G.A., 2015. A diffusion tensor MRI atlas of the postmortem rhesus macaque brain. Neuroimage 117, 408–416.

Capitanio, J.P., Emborg, M.E., 2008. Contributions of non-human primates to neuroscience research. Lancet 371, 1126–1135.

Caspers, S., Eickhoff, S.B., Rick, T., von Kapri, A., Kuhlen, T., Huang, R., Shah, N.J., Zilles, K., 2011. Probabilistic fibre tract analysis of cytoarchitectonically defined human inferior parietal lobule areas reveals similarities to macaques. Neuroimage 58, 362–380.

Catani, M., Jones, D.K., Donato, R., Ffytche, D.H., 2003. Occipito-temporal connections in the human brain. Brain 126, 2093–2107.

Cauda, F., Geminiani, G., D'Agata, F., Sacco, K., Duca, S., Bagshaw, A.P., Cavanna, A.E., 2010. Functional connectivity of the posteromedial cortex. PLoS One 5.

Cavanna, A.E., Trimble, M.R., 2006. The precuneus: a review of its functional anatomy and behavioural correlates. Brain 129, 564–583.

Cieslik, E.C., Zilles, K., Caspers, S., Roski, C., Kellermann, T.S., Jakobs, O., Langner, R., Laird, A.R., Fox, P.T., Eickhoff, S.B., 2013. Is there "one" DLPFC in cognitive action control? Evidence for heterogeneity from co-activation-based parcellation. Cerebr. Cortex 23, 2677–2689.

Clos, M., Amunts, K., Laird, A.R., Fox, P.T., Eickhoff, S.B., 2013. Tackling the multifunctional nature of Broca's region meta-analytically: co-activation-based parcellation of area 44. Neuroimage 83, 174–188.

Coalson, T.S., Van Essen, D.C., Glasser, M.F., 2018. The impact of traditional neuroimaging methods on the spatial localization of cortical areas. Proc. Natl. Acad. Sci. U. S. A. 115, E6356–E6365.

Croxson, P.L., Forkel, S.J., Cerliani, L., Thiebaut de Schotten, M., 2018. Structural variability across the primate brain: a cross-species comparison. Cerebr. Cortex 28, 3829–3841.

Croxson, P.L., Johansen-Berg, H., Behrens, T.E., Robson, M.D., Pinsk, M.A., Gross, C.G., Richter, W., Richter, M.C., Kastner, S., Rushworth, M.F., 2005. Quantitative investigation of connections of the prefrontal cortex in the human and macaque using probabilistic diffusion tractography. J. Neurosci. 25, 8854–8866.

Culham, J.C., Brandt, S.A., Cavanagh, P., Kanwisher, N.G., Dale, A.M., Tootell, R.B., 1998. Cortical fMRI activation produced by attentive tracking of moving targets. J. Neurophysiol. 80, 2657–2670.

Damoiseaux, J.S., Greicius, M.D., 2009. Greater than the sum of its parts: a review of studies combining structural connectivity and resting-state functional connectivity. Brain Struct. Funct. 213, 525–533.

Deco, G., McIntosh, A.R., Shen, K., Hutchison, R.M., Menon, R.S., Everling, S., Hagmann, P., Jirsa, V.K., 2014. Identification of optimal structural connectivity using functional connectivity and neural modeling. J. Neurosci. 34, 7910–7916.

Deco, G., Ponce-Alvarez, A., Mantini, D., Romani, G.L., Hagmann, P., Corbetta, M., 2013. Resting-state functional connectivity emerges from structurally and dynamically shaped slow linear fluctuations. J. Neurosci. 33, 11239–11252.

Deen, B., Pitskel, N.B., Pelphrey, K.A., 2011. Three systems of insular functional connectivity identified with cluster analysis. Cerebr. Cortex 21, 1498–1506.

Desai, R., Liebenthal, E., Possing, E.T., Waldron, E., Binder, J.R., 2005. Volumetric vs. surface-based alignment for localization of auditory cortex activation. Neuroimage 26, 1019–1029.

Desikan, R.S., Segonne, F., Fischl, B., Quinn, B.T., Dickerson, B.C., Blacker, D., Buckner, R.L., Dale, A.M., Maguire, R.P., Hyman, B.T., Albert, M.S., Killiany, R.J., 2006. An automated labeling system for subdividing the human cerebral cortex on MRI scans into gyral based regions of interest. Neuroimage 31, 968–980.

Dice, L.R., 1945. Measures of the amount of ecologic association between species. Ecology 26, 297–302.

Donahue, C.J., Glasser, M.F., Preuss, T.M., Rilling, J.K., Van Essen, D.C., 2018. Quantitative assessment of prefrontal cortex in humans relative to nonhuman primates. Proc. Natl. Acad. Sci. U. S. A. 115, E5183–E5192.

Draganski, B., Kherif, F., Kloppel, S., Cook, P.A., Alexander, D.C., Parker, G.J., Deichmann, R., Ashburner, J., Frackowiak, R.S., 2008. Evidence for segregated and integrative connectivity patterns in the human Basal Ganglia. J. Neurosci. 28, 7143–7152.

Eickhoff, S.B., Bzdok, D., Laird, A.R., Kurth, F., Fox, P.T., 2012. Activation likelihood estimation meta-analysis revisited. Neuroimage 59, 2349–2361.

Eickhoff, S.B., Bzdok, D., Laird, A.R., Roski, C., Caspers, S., Zilles, K., Fox, P.T., 2011. Co-activation patterns distinguish cortical modules, their connectivity and functional differentiation. Neuroimage 57, 938–949.

Eickhoff, S.B., Jbabdi, S., Caspers, S., Laird, A.R., Fox, P.T., Zilles, K., Behrens, T.E., 2010. Anatomical and functional connectivity of cytoarchitectonic areas within the human parietal operculum. J. Neurosci. 30, 6409–6421.

Eickhoff, S.B., Laird, A.R., Grefkes, C., Wang, L.E., Zilles, K., Fox, P.T., 2009. Coordinate-based activation likelihood estimation meta-analysis of neuroimaging data: a random-effects approach based on empirical estimates of spatial uncertainty. Hum. Brain Mapp. 30, 2907–2926.

Eickhoff, S.B., Stephan, K.E., Mohlberg, H., Grefkes, C., Fink, G.R., Amunts, K., Zilles, K., 2005. A new SPM toolbox for combining probabilistic cytoarchitectonic maps and functional imaging data. Neuroimage 25, 1325–1335.

Fan, L., Li, H., Zhuo, J., Zhang, Y., Wang, J., Chen, L., Yang, Z., Chu, C., Xie, S., Laird, A.R., Fox, P.T., Eickhoff, S.B., Yu, C., Jiang, T., 2016. The human brainnetome atlas: a new brain atlas based on connectional architecture. Cerebr. Cortex 26, 3508–3526.

Fan, L., Wang, J., Zhang, Y., Han, W., Yu, C., Jiang, T., 2014. Connectivity-based parcellation of the human temporal pole using diffusion tensor imaging. Cerebr. Cortex 24, 3365–3378.

Geyer, S., Matelli, M., Luppino, G., Zilles, K., 2000. Functional neuroanatomy of the primate isocortical motor system. Anat. Embryol. 202, 443–474.

Gil-da-Costa, R., Martin, A., Lopes, M.A., Munoz, M., Fritz, J.B., Braun, A.R., 2006. Species-specific calls activate homologs of Broca's and Wernicke's areas in the macaque. Nat. Neurosci. 9, 1064–1070.

Glasser, M.F., Coalson, T.S., Robinson, E.C., Hacker, C.D., Harwell, J., Yacoub, E., Ugurbil, K., Andersson, J., Beckmann, C.F., Jenkinson, M., Smith, S.M., Van Essen, D.C., 2016. A multi-modal parcellation of human cerebral cortex. Nature 536, 171–178.
Glasser, M.F., Sotiropoulos, S.N., Wilson, J.A., Coalson, T.S., Fischl, B., Andersson, J.L., Xu, J., Jbabdi, S., Webster, M., Polimeni, J.R., Van Essen, D.C., Jenkinson, M., Consortium, W.U.-M.H., 2013. The minimal preprocessing pipelines for the Human Connectome Project. Neuroimage 80, 105–124.
Goldman-Rakic, P.S., 1987. Development of cortical circuitry and cognitive function. Child Dev. 58, 601–622.
Gong, G., He, Y., Concha, L., Lebel, C., Gross, D.W., Evans, A.C., Beaulieu, C., 2009. Mapping anatomical connectivity patterns of human cerebral cortex using in vivo diffusion tensor imaging tractography. Cerebr. Cortex 19, 524–536.
Gregoriou, G.G., Rossi, A.F., Ungerleider, L.G., Desimone, R., 2014. Lesions of prefrontal cortex reduce attentional modulation of neuronal responses and synchrony in V4. Nat. Neurosci. 17, 1003–1011.
Greicius, M.D., Krasnow, B., Reiss, A.L., Menon, V., 2003. Functional connectivity in the resting brain: a network analysis of the default mode hypothesis. Proc. Natl. Acad. Sci. U. S. A. 100, 253–258.
Haber, S.N., Knutson, B., 2010. The reward circuit: linking primate anatomy and human imaging. Neuropsychopharmacology 35, 4–26.
Hackett, T.A., Preuss, T.M., Kaas, J.H., 2001. Architectonic identification of the core region in auditory cortex of macaques, chimpanzees, and humans. J. Comp. Neurol. 441, 197–222.
Hagmann, P., Cammoun, L., Gigandet, X., Meuli, R., Honey, C.J., Wedeen, V.J., Sporns, O., 2008. Mapping the structural core of human cerebral cortex. PLoS Biol. 6, e159.
Hagmann, P., Jonasson, L., Maeder, P., Thiran, J.P., Wedeen, V.J., Meuli, R., 2006. Understanding diffusion MR imaging techniques: from scalar diffusion-weighted imaging to diffusion tensor imaging and beyond. Radiographics 26 (Suppl. 1), S205–S223.
Hanakawa, T., Immisch, I., Toma, K., Dimyan, M.A., Van Gelderen, P., Hallett, M., 2003. Functional properties of brain areas associated with motor execution and imagery. J. Neurophysiol. 89, 989–1002.
Hill, J., Inder, T., Neil, J., Dierker, D., Harwell, J., Van Essen, D., 2010. Similar patterns of cortical expansion during human development and evolution. Proc. Natl. Acad. Sci. U. S. A. 107, 13135–13140.
Honey, C.J., Sporns, O., Cammoun, L., Gigandet, X., Thiran, J.P., Meuli, R., Hagmann, P., 2009. Predicting human resting-state functional connectivity from structural connectivity. Proc. Natl. Acad. Sci. U. S. A. 106, 2035–2040.
Hutchison, R.M., Culham, J.C., Flanagan, J.R., Everling, S., Gallivan, J.P., 2015. Functional subdivisions of medial parieto-occipital cortex in humans and nonhuman primates using resting-state fMRI. Neuroimage 116, 10–29.
Hutton, C., Bork, A., Josephs, O., Deichmann, R., Ashburner, J., Turner, R., 2002. Image distortion correction in fMRI: a quantitative evaluation. Neuroimage 16, 217–240.
Johansen-Berg, H., Behrens, T.E., Robson, M.D., Drobnjak, I., Rushworth, M.F., Brady, J.M., Smith, S.M., Higham, D.J., Matthews, P.M., 2004. Changes in connectivity profiles define functionally distinct regions in human medial frontal cortex. Proc. Natl. Acad. Sci. U. S. A. 101, 13335–13340.
Knauff, M., Fangmeier, T., Ruff, C.C., Johnson-Laird, P.N., 2003. Reasoning, models, and images: behavioral measures and cortical activity. J. Cogn. Neurosci. 15, 559–573.
Lacquaniti, F., Guigon, E., Bianchi, L., Ferraina, S., Caminiti, R., 1995. Representing spatial information for limb movement: role of area 5 in the monkey. Cerebr. Cortex 5, 391–409.
Laird, A.R., Eickhoff, S.B., Fox, P.M., Uecker, A.M., Ray, K.L., Saenz Jr., J.J., McKay, D.R., Bzdok, D., Laird, R.W., Robinson, J.L., Turner, J.A., Turkeltaub, P.E., Lancaster, J.L., Fox, P.T., 2011. The BrainMap strategy for standardization, sharing, and meta-analysis of neuroimaging data. BMC Res. Notes 4, 349.
Laird, A.R., Eickhoff, S.B., Kurth, F., Fox, P.M., Uecker, A.M., Turner, J.A., Robinson, J.L., Lancaster, J.L., Fox, P.T., 2009. ALE meta-analysis workflows via the brainmap database: progress towards a probabilistic functional brain atlas. Front. Neuroinf. 3, 23.
Laird, A.R., Eickhoff, S.B., Rottschy, C., Bzdok, D., Ray, K.L., Fox, P.T., 2013. Networks of task co-activations. Neuroimage 80, 505–514.
Leichnetz, G.R., 2001. Connections of the medial posterior parietal cortex (area 7m) in the monkey. Anat. Rec. 263, 215–236.
Marconi, B., Genovesio, A., Battaglia-Mayer, A., Ferraina, S., Squatrito, S., Molinari, M., Lacquaniti, F., Caminiti, R., 2001. Eye-hand coordination during reaching. I. Anatomical relationships between parietal and frontal cortex. Cerebr. Cortex 11, 513–527.
Margulies, D.S., Vincent, J.L., Kelly, C., Lohmann, G., Uddin, L.Q., Biswal, B.B., Villringer, A., Castellanos, F.X., Milham, M.P., Petrides, M., 2009. Precuneus shares intrinsic functional architecture in humans and monkeys. Proc. Natl. Acad. Sci. U. S. A. 106, 20069–20074.
Markov, N.T., Misery, P., Falchier, A., Lamy, C., Vezoli, J., Quilodran, R., Gariel, M.A., Giroud, P., Ercsey-Ravasz, M., Pilaz, L.J., Huissoud, C., Barone, P., Dehay, C., Toroczkai, Z., Van Essen, D.C., Kennedy, H., Knoblauch, K., 2011. Weight consistency specifies regularities of macaque cortical networks. Cerebr. Cortex 21, 1254–1272.
Mars, R.B., Jbabdi, S., Sallet, J., O'Reilly, J.X., Croxson, P.L., Olivier, E., Noonan, M.P., Bergmann, C., Mitchell, A.S., Baxter, M.G., Behrens, T.E., Johansen-Berg, H., Tomassini, V., Miller, K.L., Rushworth, M.F., 2011. Diffusion-weighted imaging tractography-based parcellation of the human parietal cortex and comparison with human and macaque resting-state functional connectivity. J. Neurosci. 31, 4087–4100.
Mars, R.B., Sallet, J., Neubert, F.X., Rushworth, M.F., 2013. Connectivity profiles reveal the relationship between brain areas for social cognition in human and monkey temporoparietal cortex. Proc. Natl. Acad. Sci. U. S. A. 110, 10806–10811.
Mars, R.B., Verhagen, L., Gladwin, T.E., Neubert, F.X., Sallet, J., Rushworth, M.F., 2016. Comparing brains by matching connectivity profiles. Neurosci. Biobehav. Rev. 60, 90–97.
Mesulam, M.M., Mufson, E.J., 1982. Insula of the old world monkey. III: efferent cortical output and comments on function. J. Comp. Neurol. 212, 38–52.
Morecraft, R.J., Cipolloni, P.B., Stilwell-Morecraft, K.S., Gedney, M.T., Pandya, D.N., 2004. Cytoarchitecture and cortical connections of the posterior cingulate and adjacent somatosensory fields in the rhesus monkey. J. Comp. Neurol. 469, 37–69.
Morecraft, R.J., Stilwell-Morecraft, K.S., Cipolloni, P.B., Ge, J., McNeal, D.W., Pandya, D.N., 2012. Cytoarchitecture and cortical connections of the anterior cingulate and adjacent somatomotor fields in the rhesus monkey. Brain Res. Bull. 87, 457–497.
Mufson, E.J., Mesulam, M.M., 1982. Insula of the old world monkey. II: afferent cortical input and comments on the claustrum. J. Comp. Neurol. 212, 23–37.
Nakahara, K., Hayashi, T., Konishi, S., Miyashita, Y., 2002. Functional MRI of macaque monkeys performing a cognitive set-shifting task. Science 295, 1532–1536.
Neubert, F.X., Mars, R.B., Sallet, J., Rushworth, M.F., 2015. Connectivity reveals relationship of brain areas for reward-guided learning and decision making in human and monkey frontal cortex. Proc. Natl. Acad. Sci. U. S. A. 112, E2695–E2704.
Neubert, F.X., Mars, R.B., Thomas, A.G., Sallet, J., Rushworth, M.F., 2014. Comparison of human ventral frontal cortex areas for cognitive control and language with areas in monkey frontal cortex. Neuron 81, 700–713.
Operto, G., Bulot, R., Anton, J.L., Coulon, O., 2008. Projection of fMRI data onto the cortical surface using anatomically-informed convolution kernels. Neuroimage 39, 127–135.
Owen, A.M., McMillan, K.M., Laird, A.R., Bullmore, E., 2005. N-back working memory paradigm: a meta-analysis of normative functional neuroimaging studies. Hum. Brain Mapp. 25, 46–59.
Pandya, D.N., Seltzer, B., 1982. Intrinsic connections and architectonics of posterior parietal cortex in the rhesus monkey. J. Comp. Neurol. 204, 196–210.
Parvizi, J., Van Hoesen, G.W., Buckwalter, J., Damasio, A., 2006. Neural connections of the posteromedial cortex in the macaque. Proc. Natl. Acad. Sci. U. S. A. 103, 1563–1568.
Passingham, R.E., Stephan, K.E., Kotter, R., 2002. The anatomical basis of functional localization in the cortex. Nat. Rev. Neurosci. 3, 606–616.
Passingham, R.E., Toni, I., Schluter, N., Rushworth, M.F., 1998. How do visual instructions influence the motor system? Novartis Found. Symp. 218, 129–141. ; discussion 141-126.
Picard, N., Strick, P.L., 2001. Imaging the premotor areas. Curr. Opin. Neurobiol. 11, 663–672.
Raichle, M.E., MacLeod, A.M., Snyder, A.Z., Powers, W.J., Gusnard, D.A., Shulman, G.L., 2001. A default mode of brain function. Proc. Natl. Acad. Sci. U. S. A. 98, 676–682.
Robinson, J.L., Laird, A.R., Glahn, D.C., Lovallo, W.R., Fox, P.T., 2010. Metaanalytic connectivity modeling: delineating the functional connectivity of the human amygdala. Hum. Brain Mapp. 31, 173–184.
Rohlfing, T., Kroenke, C.D., Sullivan, E.V., Dubach, M.F., Bowden, D.M., Grant, K.A., Pfefferbaum, A., 2012. The INIA19 template and NeuroMaps atlas for primate brain image parcellation and spatial normalization. Front. Neuroinf. 6, 27.
Rosene, D.L., Van Hoesen, G.W., 1977. Hippocampal efferents reach widespread areas of cerebral cortex and amygdala in the rhesus monkey. Science 198, 315–317.
Rottschy, C., Caspers, S., Roski, C., Reetz, K., Dogan, I., Schulz, J.B., Zilles, K., Laird, A.R., Fox, P.T., Eickhoff, S.B., 2013. Differentiated parietal connectivity of frontal regions for "what" and "where" memory. Brain Struct. Funct. 218, 1551–1567.
Sallet, J., Mars, R.B., Noonan, M.P., Neubert, F.X., Jbabdi, S., O'Reilly, J.X., Filippini, N., Thomas, A.G., Rushworth, M.F., 2013. The organization of dorsal frontal cortex in humans and macaques. J. Neurosci. 33, 12255–12274.
Saunders, R.C., Rosene, D.L., 1988. A comparison of the efferents of the amygdala and the hippocampal formation in the rhesus monkey: I. Convergence in the entorhinal, prorhinal, and perirhinal cortices. J. Comp. Neurol. 271, 153–184.
Saunders, R.C., Rosene, D.L., Van Hoesen, G.W., 1988. Comparison of the efferents of the amygdala and the hippocampal formation in the rhesus monkey: II. Reciprocal and non-reciprocal connections. J. Comp. Neurol. 271, 185–207.
Saygin, Z.M., Osher, D.E., Norton, E.S., Youssoufian, D.A., Beach, S.D., Feather, J., Gaab, N., Gabrieli, J.D., Kanwisher, N., 2016. Connectivity precedes function in the development of the visual word form area. Nat. Neurosci. 19, 1250–1255.
Scheperjans, F., Eickhoff, S.B., Homke, L., Mohlberg, H., Hermann, K., Amunts, K., Zilles, K., 2008a. Probabilistic maps, morphometry, and variability of cytoarchitectonic areas in the human superior parietal cortex. Cerebr. Cortex 18, 2141–2157.
Scheperjans, F., Hermann, K., Eickhoff, S.B., Amunts, K., Schleicher, A., Zilles, K., 2008b. Observer-independent cytoarchitectonic mapping of the human superior parietal cortex. Cerebr. Cortex 18, 846–867.
Simon, O., Mangin, J.F., Cohen, L., Le Bihan, D., Dehaene, S., 2002. Topographical layout of hand, eye, calculation, and language-related areas in the human parietal lobe. Neuron 33, 475–487.
Squire, L.R., 1992. Memory and the hippocampus: a synthesis from findings with rats, monkeys, and humans. Psychol. Rev. 99, 195–231.
Suchan, B., Yaguez, L., Wunderlich, G., Canavan, A.G., Herzog, H., Tellmann, L., Homberg, V., Seitz, R.J., 2002. Hemispheric dissociation of visual-pattern processing and visual rotation. Behav. Brain Res. 136, 533–544.
Suzuki, W.A., Amaral, D.G., 1994. Topographic organization of the reciprocal connections between the monkey entorhinal cortex and the perirhinal and parahippocampal cortices. J. Neurosci. 14, 1856–1877.

Szczepanski, S.M., Pinsk, M.A., Douglas, M.M., Kastner, S., Saalmann, Y.B., 2013. Functional and structural architecture of the human dorsal frontoparietal attention network. Proc. Natl. Acad. Sci. U. S. A. 110, 15806–15811.
Tomassini, V., Jbabdi, S., Klein, J.C., Behrens, T.E., Pozzilli, C., Matthews, P.M., Rushworth, M.F., Johansen-Berg, H., 2007. Diffusion-weighted imaging tractography-based parcellation of the human lateral premotor cortex identifies dorsal and ventral subregions with anatomical and functional specializations. J. Neurosci. 27, 10259–10269.
Touroutoglou, A., Bliss-Moreau, E., Zhang, J., Mantini, D., Vanduffel, W., Dickerson, B.C., Barrett, L.F., 2016. A ventral salience network in the macaque brain. Neuroimage 132, 190–197.
Tsao, D.Y., Moeller, S., Freiwald, W.A., 2008. Comparing face patch systems in macaques and humans. Proc. Natl. Acad. Sci. U. S. A. 105, 19514–19519.
Tucholka, A., Fritsch, V., Poline, J.B., Thirion, B., 2012. An empirical comparison of surface-based and volume-based group studies in neuroimaging. Neuroimage 63, 1443–1453.
Turkeltaub, P.E., Eickhoff, S.B., Laird, A.R., Fox, M., Wiener, M., Fox, P., 2012. Minimizing within-experiment and within-group effects in activation likelihood estimation meta-analyses. Hum. Brain Mapp. 33, 1–13.
Van Essen, D.C., Smith, S.M., Barch, D.M., Behrens, T.E., Yacoub, E., Ugurbil, K., Consortium, W.U.-M.H., 2013. The Wu-minn human connectome Project: an overview. Neuroimage 80, 62–79.
Vincent, J.L., Kahn, I., Van Essen, D.C., Buckner, R.L., 2010. Functional connectivity of the macaque posterior parahippocampal cortex. J. Neurophysiol. 103, 793–800.
Wang, J., Fan, L., Wang, Y., Xu, W., Jiang, T., Fox, P.T., Eickhoff, S.B., Yu, C., Jiang, T., 2015a. Determination of the posterior boundary of Wernicke's area based on multimodal connectivity profiles. Hum. Brain Mapp. 36, 1908–1924.
Wang, J., Fan, L., Zhang, Y., Liu, Y., Jiang, D., Zhang, Y., Yu, C., Jiang, T., 2012. Tractography-based parcellation of the human left inferior parietal lobule. Neuroimage 63, 641–652.
Wang, J., Feng, X., Wu, J., Xie, S., Li, L., Xu, L., Zhang, Y., Ren, X., Hu, Z., Lv, L., Hu, X., Jiang, T., 2018. Alterations of gray matter volume and white matter integrity in maternal deprivation monkeys. Neuroscience 384, 14–20.
Wang, J., Wei, Q., Bai, T., Zhou, X., Sun, H., Becker, B., Tian, Y., Wang, K., Kendrick, K., 2017b. Electroconvulsive therapy selectively enhanced feedforward connectivity from fusiform face area to amygdala in major depressive disorder. Soc. Cognit. Affect Neurosci. 12, 1983–1992.
Wang, J., Wei, Q., Yuan, X., Jiang, X., Xu, J., Zhou, X., Tian, Y., Wang, K., 2017c. Local functional connectivity density is closely associated with the response of electroconvulsive therapy in major depressive disorder. J. Affect. Disord. 225, 658–664.
Wang, J., Xie, S., Guo, X., Becker, B., Fox, P.T., Eickhoff, S.B., Jiang, T., 2017d. Correspondent functional topography of the human left inferior parietal lobule at rest and under task revealed using resting-state fMRI and coactivation based parcellation. Hum. Brain Mapp. 38, 1659–1675.
Wang, J., Yang, Y., Fan, L., Xu, J., Li, C., Liu, Y., Fox, P.T., Eickhoff, S.B., Yu, C., Jiang, T., 2015b. Convergent functional architecture of the superior parietal lobule unraveled with multimodal neuroimaging approaches. Hum. Brain Mapp. 36, 238–257.
Wang, J., Zhang, J., Rong, M., Wei, X., Zheng, D., Fox, P.T., Eickhoff, S.B., Jiang, T., 2016. Functional topography of the right inferior parietal lobule structured by anatomical connectivity profiles. Hum. Brain Mapp. 37, 4316–4332.
Wang, J., Zuo, Z., Xie, S., Miao, Y., Ma, Y., Zhao, X., Jiang, T., 2018e. Parcellation of macaque cortex with anatomical connectivity profiles. Brain Topogr. 31, 161–173.
Wenderoth, N., Debaere, F., Sunaert, S., Swinnen, S.P., 2005. The role of anterior cingulate cortex and precuneus in the coordination of motor behaviour. Eur. J. Neurosci. 22, 235–246.
Wu, H., Sun, H., Wang, C., Yu, L., Li, Y., Peng, H., Lu, X., Hu, Q., Ning, Y., Jiang, T., Xu, J., Wang, J., 2017. Abnormalities in the structural covariance of emotion regulation networks in major depressive disorder. J. Psychiatr. Res. 84, 237–242.
Wu, Y., Wang, J., Zhang, Y., Zheng, D., Zhang, J., Rong, M., Wu, H., Wang, Y., Zhou, K., Jiang, T., 2016a. The neuroanatomical basis for posterior superior parietal lobule control lateralization of visuospatial attention. Front. Neuroanat. 10, 32.
Wu, Y., Zhang, Y., Liu, Y., Liu, J., Duan, Y., Wei, X., Zhuo, J., Li, K., Zhang, X., Yu, C., Wang, J., Jiang, T., 2016b. Distinct changes in functional connectivity in posteromedial cortex subregions during the progress of Alzheimer's disease. Front. Neuroanat. 10.
Xu, J., Wang, J., Fan, L., Li, H., Zhang, W., Hu, Q., Jiang, T., 2015. Tractography-based parcellation of the human middle temporal gyrus. Sci. Rep. 5, 18883.
Xu, T., Falchier, A., Sullivan, E.L., Linn, G., Ramirez, J.S.B., Ross, D., Feczko, E., Opitz, A., Bagley, J., Sturgeon, D., Earl, E., Miranda-Dominguez, O., Perrone, A., Craddock, R.C., Schroeder, C.E., Colcombe, S., Fair, D.A., Milham, M.P., 2018. Delineating the macroscale Areal organization of the macaque cortex in vivo. Cell Rep. 23, 429–441.
Yang, Y., Fan, L., Chu, C., Zhuo, J., Wang, J., Fox, P.T., Eickhoff, S.B., Jiang, T., 2016. Identifying functional subdivisions in the human brain using meta-analytic activation modeling-based parcellation. Neuroimage 124, 300–309.
Zhang, D., Snyder, A.Z., Shimony, J.S., Fox, M.D., Raichle, M.E., 2010. Noninvasive functional and structural connectivity mapping of the human thalamocortical system. Cerebr. Cortex 20, 1187–1194.
Zhang, S., Li, C.S., 2012. Functional connectivity mapping of the human precuneus by resting state fMRI. Neuroimage 59, 3548–3562.
Zhang, W., Wang, J., Fan, L., Zhang, Y., Fox, P.T., Eickhoff, S.B., Yu, C., Jiang, T., 2016. Functional organization of the fusiform gyrus revealed with connectivity profiles. Hum. Brain Mapp. 37, 3003–3016.
Zhang, Y., Fan, L., Zhang, Y., Wang, J., Zhu, M., Zhang, Y., Yu, C., Jiang, T., 2014. Connectivity-based parcellation of the human posteromedial cortex. Cerebr. Cortex 24, 719–727.